A similar replacement of the active subset is not apparent in the dentate gyrus, which suggests that the change in the CA3 code is triggered by direct projections from entorhinal grid cells to the CA3 (*32*).

Pattern separation in the dentate gyrus is thus different from separation processes in the cerebellum (*10*, *11*), where signals from the brain stem spread out on a layer of granule cells whose cell numbers exceed those of the input layer by a factor of several million. The number of granule cells in the dentate gyrus and pyramidal cells in the CA3 only marginally outnumbers the projection neurons from layer II of the entorhinal cortex [in the rat, 1,000,000, 300,000 and 200,000, respectively (*15*, *35*, *36*)], which suggests that the same hippocampal cells must participate in many representations even when the population activity is sparse (*13*, *14*). In such networks, orthogonalization of coincidence patterns may be more effective.

The decorrelated firing of the dentate cells contrasts with the invariant discharge structure of grid cells upstream in the medial entorhinal cortex (*30*–*32*) (Fig. 4). The reduction in spatiotemporal coincidence could be derived from the lateral entorhinal cortex, but not by a straightforward relay mechanism, because cells in this area do not exhibit reliable place modulation (*37*). It is thus likely that many of the underlying computations take place within the dentate gyrus itself. The use of a dedicated neuronal population for orthogonalization of small differences in input to the CA fields enables the hippocampal network to encode the full variety of experience in a more diversified manner than what could be accomplished with attractor networks alone.

References and Notes

1. B. L. McNaughton, L. Nadel, in *Neuroscience and Connectionist Theory*, M. A. Gluck and D. E. Rumelhart, Eds. (Lawrence Erlbaum, Hillsdale, NJ, 1989), pp. 1–63.
2. A. Treves, E. T. Rolls, *Hippocampus* **2**, 189 (1992).
3. R. C. O'Reilly, J. L. McClelland, *Hippocampus* **4**, 661 (1994).
4. P. E. Gilbert, R. P. Kesner, I. Lee, *Hippocampus* **11**, 626 (2001).
5. D. Marr, *Philos. Trans. R. Soc. Lond. B Biol. Sci.* **262**, 23 (1971).
6. M. E. Hasselmo, E. Schnell, E. Barkai, *J. Neurosci.* **15**, 5249 (1995).
7. M. Tsodyks, *Hippocampus* **9**, 481 (1999).
8. K. Nakazawa *et al.*, *Science* **297**, 211 (2002).
9. I. Lee, D. Yoganarasimha, G. Rao, J. J. Knierim, *Nature* **430**, 456 (2004).
10. D. Marr, *J. Physiol.* **202**, 437 (1969).
11. J. Albus, *Math. Biosci.* **10**, 25 (1971).
12. P. Chadderton, T. W. Margrie, M. Hausser, *Nature* **428**, 856 (2004).
13. M. W. Jung, B. L. McNaughton, *Hippocampus* **3**, 165 (1993).
14. M. K. Chawla *et al.*, *Hippocampus* **15**, 579 (2005).
15. D. G. Amaral, N. Ishizuka, B. Claiborne, *Prog. Brain Res.* **83**, 1 (1990).
16. J. O'Keefe, J. Dostrovsky, *Brain Res.* **34**, 171 (1971).
17. R. U. Muller, J. L. Kubie, J. B. Ranck Jr., *J. Neurosci.* **7**, 1935 (1987).
18. R. U. Muller, J. L. Kubie, *J. Neurosci.* **7**, 1951 (1987).
19. G. J. Quirk, R. U. Muller, J. L. Kubie, *J. Neurosci.* **10**, 2008 (1990).
20. E. Bostock, R. U. Muller, J. L. Kubie, *Hippocampus* **1**, 193 (1991).
21. E. J. Markus *et al.*, *J. Neurosci.* **15**, 7079 (1995).
22. C. Lever, T. Wills, F. Cacucci, N. Burgess, J. O'Keefe, *Nature* **416**, 90 (2002).
23. T. J. Wills, C. Lever, F. Cacucci, N. Burgess, J. O'Keefe, *Science* **308**, 873 (2005).
24. S. Leutgeb *et al.*, *Science* **309**, 619 (2005).
25. Materials and Methods and other supporting material are available on *Science* Online.
26. J. K. Leutgeb *et al.*, *Neuron* **48**, 345 (2005).
27. D. A. Henze, L. Wittner, G. Buzsáki, *Nat. Neurosci.* **5**, 790 (2002).
28. K. D. Harris, J. Csicsvari, H. Hirase, G. Dragoi, G. Buzsáki, *Nature* **424**, 552 (2003).
29. R. M. Hayman, S. Chakraborty, M. I. Anderson, K. J. Jeffery, *Eur. J. Neurosci.* **18**, 2825 (2003).
30. M. Fyhn, S. Molden, M. P. Witter, E. I. Moser, M.-B. Moser, *Science* **305**, 1258 (2004).
31. T. Hafting, M. Fyhn, S. Molden, M.-B. Moser, E. I. Moser, *Nature* **436**, 801 (2005).
32. M. H. Fyhn, T. F. Hafting, A. Treves, E. I. Moser, M.-B. Moser, *Nature,* in press.
33. S. Leutgeb, J. K. Leutgeb, A. Treves, M.-B. Moser, E. I. Moser, *Science* **305**, 1295 (2004).
34. A. Vazdarjanova, J. F. Guzowski, *J. Neurosci.* **24**, 6489 (2004).
35. P. R. Rapp, P. S. Deroche, Y. Mao, R. D. Burwell, *Cereb. Cortex* **12**, 1171 (2002).
36. B. D. Boss, G. M. Peterson, W. M. Cowan, *Brain Res.* **338**, 144 (1985).
37. E. L. Hargreaves, G. Rao, I. Lee, J. J. Knierim, *Science* **308**, 1792 (2005).

38. We thank A. Treves, C. A. Barnes, and M. R. Mehta for discussion and A. M. Amundsgard, K. Haugen, K. Jenssen, E. Sjulstad, R. Skjerpeng, and H. Waade for technical assistance. This work was supported by a Centre of Excellence grant from the Norwegian Research Council.

Supporting Online Material

www.sciencemag.org/cgi/content/full/315/5814/961/DC1
Materials and Methods
SOM Text
Figs. S1 to S12
Tables S1 and S2
References

2 October 2006; accepted 15 December 2006
10.1126/science.1135801

REPORTS

Experimental Realization of Wheeler's Delayed-Choice Gedanken Experiment

Vincent Jacques,[1] E Wu,[1,2] Frédéric Grosshans,[1] François Treussart,[1] Philippe Grangier,[3] Alain Aspect,[3] Jean-François Roch[1]*

Wave-particle duality is strikingly illustrated by Wheeler's delayed-choice gedanken experiment, where the configuration of a two-path interferometer is chosen after a single-photon pulse has entered it: Either the interferometer is closed (that is, the two paths are recombined) and the interference is observed, or the interferometer remains open and the path followed by the photon is measured. We report an almost ideal realization of that gedanken experiment with single photons allowing unambiguous which-way measurements. The choice between open and closed configurations, made by a quantum random number generator, is relativistically separated from the entry of the photon into the interferometer.

Young's double-slit experiment, realized with particles sent one at a time through an interferometer, is at the heart of quantum mechanics (*1*). The striking feature is that the phenomenon of interference, interpreted as a wave following two paths simultaneously, is incompatible with our common-sense representation of a particle following one route or the other but not both. Several single-photon interference experiments (*2*–*6*) have confirmed the wave-particle duality of the light field. To understand their meaning, consider the single-photon interference experiment sketched in Fig. 1. In the closed interferometer configuration, a single-photon pulse is split by a first beamsplitter BS_{input} of a Mach-Zehnder interferometer and travels through it until a second beamsplitter BS_{output} recombines the two interfering arms. When the phase shift Φ between the two arms is varied, interference appears as a modulation of the detection probabilities at output ports 1 and 2, respectively, as $\cos^2 \Phi$ and $\sin^2 \Phi$. This result is the one expected for a wave, and as Wheeler pointed out, "[this] is evidence … that each ar-

[1]Laboratoire de Photonique Quantique et Moléculaire, Ecole Normale Supérieure de Cachan, UMR CNRS 8537, 94235 Cachan, France. [2]Key Laboratory of Optical and Magnetic Resonance Spectroscopy, East China Normal University, 200062 Shanghai, China. [3]Laboratoire Charles Fabry de l'Institut d'Optique, Campus Polytechnique, UMR CNRS 8501, 91127 Palaiseau, France.

*To whom correspondence should be addressed. E-mail: roch@physique.ens-cachan.fr

riving light quantum has arrived by both routes" (*7*). If BS_{output} is removed (the open configuration), each detector D1 or D2 on the output ports is then associated with a given path of the interferometer, and, provided one uses true single-photon light pulses, "[either] one counter goes off, or the other. Thus the photon has traveled only one route" (*7*). Such an experiment supports Bohr's statement that the behavior of a quantum system is determined by the type of measurement performed on it (*8*). Moreover, it is clear that for the two complementary measurements considered here, the corresponding experimental settings are mutually exclusive; that is, BS_{output} cannot be simultaneously present and absent.

In experiments where the choice between the two settings is made long in advance, one could reconcile Bohr's complementarity with Einstein's local conception of the physical reality. Indeed, when the photon enters the interferometer, it could have received some "hidden information" on the chosen experimental configuration and could then adjust its behavior accordingly (*9*). To rule out that too-naïve interpretation of quantum mechanical complementarity, Wheeler proposed the "delayed-choice" gedanken experiment in which the choice of which property will be observed is made after the photon has passed BS_{input}: "Thus one decides the photon shall have come by one route or by both routes after it has already done its travel" (*7*).

Since Wheeler's proposal, several delayed-choice experiments have been reported (*10*–*15*). However, none of them fully followed the original scheme, which required the use of the single-particle quantum state as well as relativistic space-like separation between the choice of interferometer configuration and the entry of the particle into the interferometer. We report the realization of such a delayed-choice experiment in a scheme close to the ideal original proposal (Fig. 1). The choice to insert or remove BS_{output} is randomly decided through the use of a quantum random number generator (QRNG). The QRNG is located close to BS_{output} and is far enough from the input so that no information about the choice can reach the photon before it passes through BS_{input}.

Our single-photon source, previously developed for quantum key distribution (*16*, *17*), is based on the pulsed, optically excited photoluminescence of a single nitrogen-vacancy (N-V) color center in a diamond nanocrystal (*18*). At the single-emitter level, these photoluminescent centers, which can be individually addressed with the use of confocal microscopy (*19*), have shown unsurpassed efficiency and photostability at room temperature (*20*, *21*). In addition, it is possible to obtain single photons with a well-defined polarization (*16*, *22*).

The delayed-choice scheme is implemented as follows. Linearly polarized single photons are sent by a polarization beamsplitter BS_{input} through an interferometer (length 48 m) with two spatially separated paths associated with orthogonal S and P polarizations (Fig. 2). The movable output beamsplitter BS_{output} consists of the combination of a half-wave plate, a polarization beamsplitter BS′, an electro-optical modulator (EOM) with its optical axis oriented at 22.5° from input polarizations, and a Wollaston prism. The two beams of the interferometer, which are spatially separated and orthogonally polarized, are first overlapped by BS′ but can still be unambiguously identified by their polarization. Then, the choice between the two interferometer configurations, closed or open, is realized with the EOM, which can be switched between two different configurations within 40 ns by means of a homebuilt fast driver (*16*): Either no voltage is applied to the EOM, or its half-wave voltage V_π is applied to it. In the first case, the situation corresponds to the removal of BS_{output} and the two paths remain uncombined (open configuration). Because the original S and P polarizations of the two paths are oriented along prism polarization eigenstates, each "click" of one detector D1 or D2 placed on the output ports is associated with a specific path (path 1 or path 2, respectively). When the V_π voltage is applied, the EOM is equivalent to a half-wave plate that rotates the input polarizations by an angle of 45°. The prism then recombines the two rotated polarizations that have traveled along different optical paths, and interference appears on the two output ports. We then have the closed interferometer configuration (*22*).

To ensure the relativistic space-like separation between the choice of the interferometer configuration and the passage of the photon at BS_{input}, we configured the EOM switching process to be randomly decided in real time by the QRNG located close to the output of the interferometer (48 m from BS_{input}). The random number is generated by sampling the amplified shot noise of a white-light beam. Shot noise is an intrinsic quantum random process, and its value at a given time cannot be predicted (*23*). The timing of the experiment ensures the required relativistic space-like separation (*22*). Then, no information about the interferometer configuration choice can reach the photon before it enters the interferometer.

The single-photon behavior was first tested using the two output detectors feeding single and

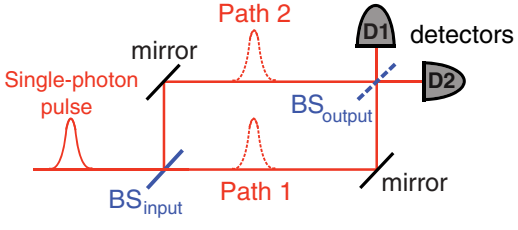

Fig. 1. Wheeler's delayed-choice gedanken experiment proposal. The choice to introduce or remove beamsplitter BS_{output} (closed or open configuration) is made only after the passage of the photon at BS_{input}, so that the photon entering the interferometer "cannot know" which of the two complementary experiments (path difference versus which-way) will be performed at the output.

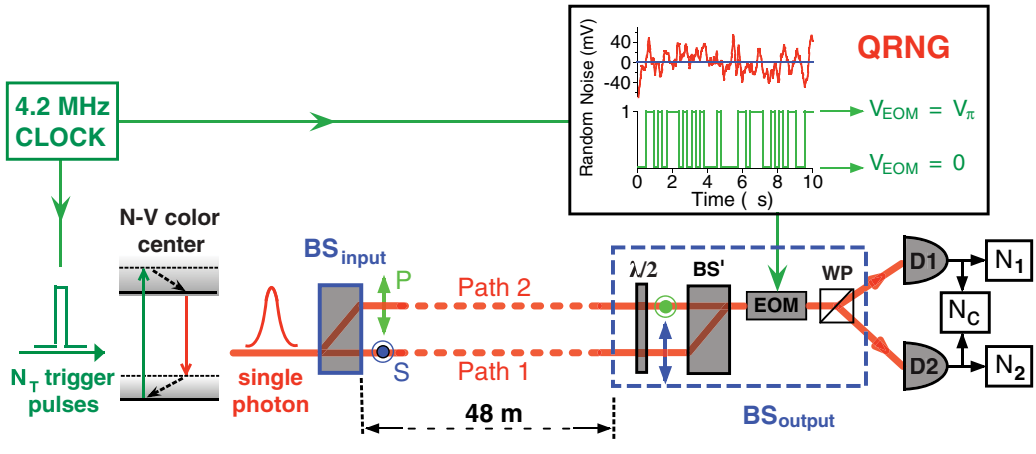

Fig. 2. Experimental realization of Wheeler's gedanken experiment. Single photons emitted by a single N-V color center are sent through a 48-m polarization interferometer, equivalent to a time of flight of about 160 ns. A binary random number 0 or 1, generated by the QRNG, drives the EOM voltage between $V = 0$ and $V = V_\pi$ within 40 ns, after an electronic delay of 80 ns. Two synchronized signals from the clock are used to trigger the single-photon emission and the QNRG. In the laboratory frame of reference, the random choice between the open and the closed configuration is made simultaneously with the entry of the photon into the interferometer. Taking advantage of the fact that the QNRG is located at the output of the interferometer, such timing ensures that the photon enters the future light cone of the random choice when it is at about the middle of the interferometer, long after passing BS_{input}.

coincidence counters with BS_{output} removed (open configuration). We used an approach similar to the one described in (*2*) and (*6*). Consider a run corresponding to N_T trigger pulses applied to the emitter, with N_1 counts detected in path 1 of the interferometer by D1, N_2 counts detected in path 2 by D2, and N_C detected coincidences corresponding to joint photodetections on D1 and D2 (Fig. 2). Any description in which light is treated as a classical wave, such as the semiclassical theory with quantized photodetectors (*24*), predicts that these numbers of counts should obey the inequality

$$\alpha = \frac{N_C \times N_T}{N_1 \times N_2} \geq 1 \qquad (1)$$

Violation of this inequality thus gives a quantitative criterion that characterizes nonclassical behavior. For a single-photon wavepacket, quantum optics predicts perfect anticorrelation (i.e., $\alpha = 0$) in agreement with the intuitive image that a single particle cannot be detected simultaneously in the two paths of the interferometer (*2*). We measured $\alpha = 0.12 \pm 0.01$, hence we are indeed close to the pure single-photon regime. The nonideal value of the α parameter is due to residual background photoluminescence of the diamond sample and to the two-phonon Raman scattering line, which both produce uncorrelated photons with Poissonian statistics (*6*).

With single-photon pulses in the open configuration, we expected each detector D1 and D2 to be unambiguously associated with a given path of the interferometer. To test this point, we evaluated the "which-way" information parameter $I = (N_1 - N_2)/(N_1 + N_2)$ (*25*–*28*) by blocking one path (e.g., path 2) and measuring the counting rates at D1 and D2. A value of I higher than 0.99 was measured, limited by detector dark counts and residual imperfections of the optical components. The same value was obtained when the other path was blocked (e.g., path 1). In the open configuration, we thus have an almost ideal which-way measurement.

The delayed-choice experiment itself is performed with the EOM randomly switched for each photon sent into the interferometer, corresponding to a random choice between the open and closed configurations. The phase shift Φ between the two interferometer arms is varied by tilting the second polarization beamsplitter BS′ with a piezoelectric actuator (PZT). For each photon, we recorded the chosen configuration, the detection events, and the PZT position. All raw data were saved in real time and were processed only after a run was completed. For each PZT position, detection events on D1 and D2 corresponding to each configuration were sorted (Fig. 3). In the closed configuration, we observed interference with 0.94 visibility. We attribute the departure from unity to an imperfect overlap of the two interfering beams. In the open configuration, interference totally disappears, as evidenced by the absence of modulation in the two output ports when the phase shift Φ was varied. We checked that in the delayed-choice configuration, parameters α and I kept the same values as measured in the preliminary tests presented above.

Our realization of Wheeler's delayed-choice gedanken experiment demonstrates that the behavior of the photon in the interferometer depends on the choice of the observable that is measured, even when that choice is made at a position and a time such that it is separated from the entrance of the photon into the interferometer by a space-like interval. In Wheeler's words, as no signal traveling at a velocity less than that of light can connect these two events, "we have a strange inversion of the normal order of time. We, now, by moving the mirror in or out have an unavoidable effect on what we have a right to say about the already past history of that photon" (*7*). Once more, we find that nature behaves in agreement with the predictions of quantum mechanics even in surprising situations where a tension with relativity seems to appear (*29*).

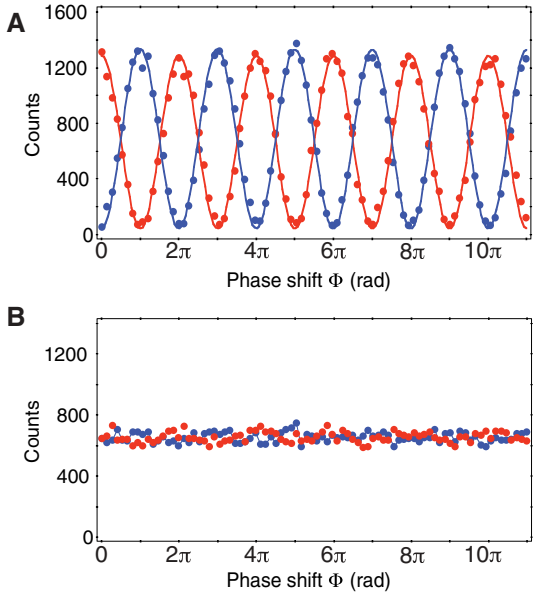

Fig. 3. Results of the delayed-choice experiment. The phase shift Φ (indicated with arbitrary origin) is varied by tilting BS′. Each point, recorded with acquisition time of 1.9 s, corresponds to the detection of about 2600 photons. The detector dark counts, 59 s^{-1} for D1 (blue points) and 70 s^{-1} for D2 (red points), have been subtracted from the data. (**A**) Cases when V_π is applied on the EOM (closed configuration); interference with 94% visibility is obtained. (**B**) Cases when no voltage is applied on the EOM (open configuration); no interference is observed and equal detection probabilities (0.50 ± 0.01) on the two output ports are measured, corresponding to full knowledge of the complementary which-way information (*I* parameter greater than 99%).

References and Notes

1. R. P. Feynman, R. B. Leighton, M. L. Sands, *Lectures on Physics* (Addison-Wesley, Reading, MA, 1965).
2. P. Grangier, G. Roger, A. Aspect, *Europhys. Lett.* **1**, 173 (1986).
3. F. Jelezko, A. Volkmer, I. Popa, K. K. Rebane, J. Wrachtrup, *Phys. Rev. A* **67**, 041802 (2003).
4. A. Zeilinger, G. Weihs, T. Jennewein, M. Aspelmeyer, *Nature* **433**, 230 (2005).
5. T. Aichele, U. Herzog, M. Scholtz, O. Benson, *AIP Conf. Proc.* **750**, 35 (2005).
6. V. Jacques *et al.*, *Eur. Phys. J. D* **35**, 561 (2005).
7. J. A. Wheeler, in *Quantum Theory and Measurement*, J. A. Wheeler, W. H. Zurek, Eds. (Princeton Univ. Press, Princeton, NJ, 1984), pp. 182–213.
8. N. Bohr, in *Quantum Theory and Measurement*, J. A. Wheeler, W. H. Zurek, Eds. (Princeton Univ. Press, Princeton, NJ, 1984), pp. 9–49.
9. G. Greenstein, A. G. Zajonc, *The Quantum Challenge* (Jones and Bartlett, Sudbury, MA, 1997).
10. C. O. Alley, O. G. Jacubowicz, W. C. Wickes, in *Proceedings of the Second International Symposium on the Foundations of Quantum Mechanics*, H. Narani, Ed. (Physics Society of Japan, Tokyo, 1987), pp. 36–47.
11. T. Hellmut, H. Walther, A. G. Zajonc, W. Schleich, *Phys. Rev. A* **72**, 2533 (1987).
12. J. Baldzuhn, E. Mohler, W. Martienssen, *Z. Phys. B* **77**, 347 (1989).
13. B. J. Lawson Daku *et al.*, *Phys. Rev. A* **54**, 5042 (1996).
14. Y.-H. Kim, R. Yu, S. P. Kulik, Y. Shih, M. O. Scully, *Phys. Rev. Lett.* **84**, 1 (2000).
15. T. Kawai *et al.*, *Nucl. Inst. Methods A* **410**, 259 (1998).
16. A. Beveratos *et al.*, *Phys. Rev. Lett.* **89**, 187901 (2002).
17. R. Alléaume *et al.*, *N. J. Phys.* **6**, 92 (2004).
18. A. Beveratos *et al.*, *Eur. Phys. J. D* **18**, 191 (2002).
19. A. Gruber *et al.*, *Science* **276**, 2012 (1997).
20. C. Kurtsiefer, S. Mayer, P. Zarda, H. Weinfurter, *Phys. Rev. Lett.* **85**, 290 (2000).
21. R. Brouri, A. Beveratos, J.-P. Poizat, P. Grangier, *Opt. Lett.* **25**, 1294 (2000).
22. See supporting material on *Science* Online.
23. H.-A. Bachor, T. C. Ralph, *A Guide to Experiments in Quantum Optics* (Wiley-VCH, Weinheim, Germany, 2004).
24. W. E. Lamb, M. O. Scully, in *Polarization, Matière et Rayonnement, Volume in Honour of A. Kastler* (Presses Universitaires de France, Paris, 1969), pp. 363–369.
25. P. Grangier, thesis, Institut d'Optique et Université Paris 11 (1986); available at http://tel.ccsd.cnrs.fr/tel-00009436.
26. B.-G. Englert, *Phys. Rev. Lett.* **77**, 2154 (1996).
27. S. Durr, T. Nonn, G. Rempe, *Phys. Rev. Lett.* **81**, 5705 (1998).
28. P. D. Schwindt, P. G. Kwiat, B.-G. Englert, *Phys. Rev. A* **60**, 4285 (1999).
29. J. S. Bell, *Speakable and Unspeakable in Quantum Mechanics* (Cambridge Univ. Press, Cambridge, 1987).

30. We thank A. Clouqueur and A. Villing for the realization of the electronics of the experiment, J.-P. Madrange for the mechanical realization of the interferometer, and A. Browaeys, L. Jacubowiez, and D. Chauvat for their constant help and many enlightening discussions. Supported by Institut Universitaire de France.

Supporting Online Material

www.sciencemag.org/cgi/content/full/315/5814/966/DC1
Materials and Methods
Figs. S1 to S4
References

13 October 2006; accepted 3 January 2007
10.1126/science.1136303

Methods

Triggered single-photon source

We use a single nitrogen-vacancy (N-V) color center in a diamond nanocrystal. The N-V centers are created by irradiation of type Ib diamond sample with high-energy electrons followed by annealing at $800°C$[1]. Under a well controlled irradiation dose, the N-V center density is small enough to allow independent addressing of a single center using standard confocal microscopy[2]. The experimental setup used to excite and spectrally characterize single color center photoluminescence is depicted on Fig. 4.

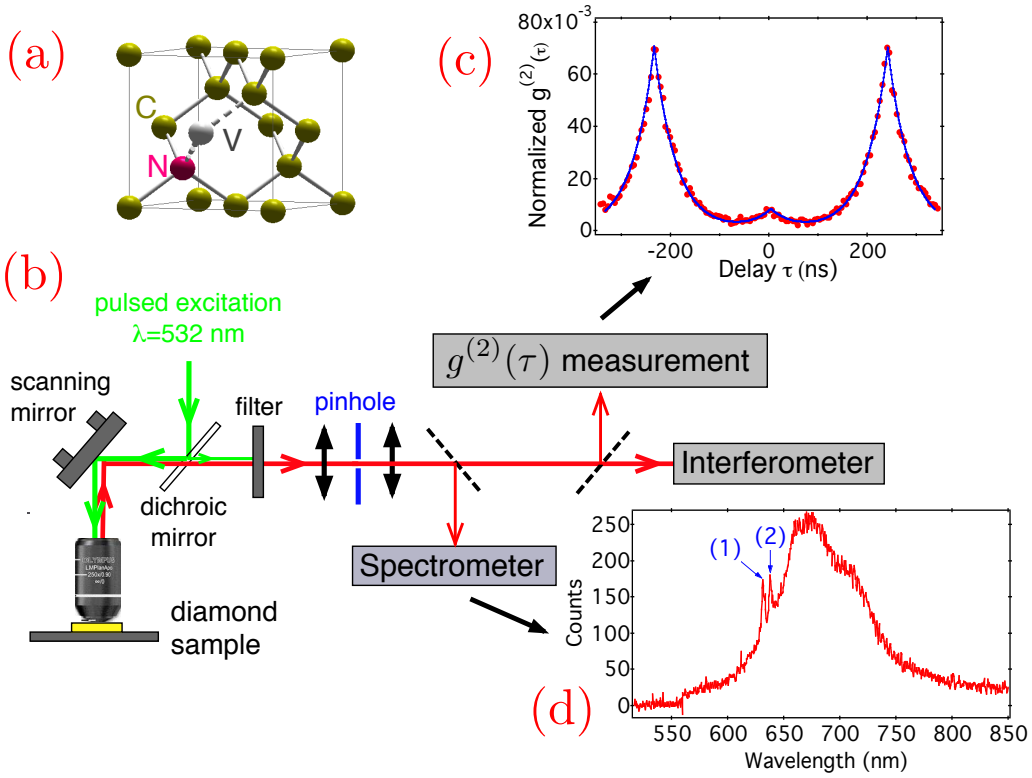

Figure 4: **(a)**-*N-V color center consisting in a substitutional Nitrogen atom (N), associated to a Vacancy (V) in an adjacent lattice site of the diamond crystalline matrix.* **(b)**- *Confocal microscopy setup. The* 532 *nm pulsed excitation laser beam is tightly focused on a diamond nanocrystals with a high numerical aperture (NA*$=0.95$*) microscope objective. The photoluminescence of the N-V color center is collected by the same objective and then spectrally filtered from residual pumping light. Following standard confocal detection scheme, the collected light is focused onto a* $100\ \mu$m *diameter pinhole. To identify a well isolated photoluminescent emitter, the sample is first raster scanned. For the center used in the experiment, a signal over background ratio of about 10 is achieved.* **(c)**-*The unicity of the emitter is then ensured by observation of antibunching in the second order correlation function* $g^{(2)}(\tau)$ *of the N-V center photoluminescence, recorded by a standard Hanbury Brown and Twiss setup. The very small remaining value at zero delay* $g^{(2)}(0) = 0.12$ *is due to background emission from the substrate and from the diamond sample in which the color center is embedded. Exponential fit of* $g^{(2)}(\tau)$ *(blue line) gives the excited level lifetime of the defect* $\tau_{\rm sp} = 44.5 \pm 0.5$ *ns.* **(d)**-*Part of the photoluminescence can be also taken to record the emission spectrum of the N-V color center. The two sharp lines (1) and (2) are respectively the two-phonon Raman scattering line of the diamond matrix associated to the excitation wavelength and the zero phonon line at 637 nm which characterizes photoluminescence of negatively charged N-V color centers.*

Excitation is done with a home-built pulsed laser at a wavelength of 532 nm [3]. The laser system delivers 800 ps pulses with energy 50 pJ, high enough to ensure efficient pumping of the color center in its excited level. The repetition rate, synchronized on a stable external clock, is set at 4.2 MHz so that successive fluorescent decays are well separated in time from each other. Single photons are thus emitted by the N-V color center at predetermined times within the accuracy of its excited state lifetime, which is about 45 ns for the center used in the experiment (see Fig.4-(c)).

[1] C. Kurtsiefer, S. Mayer, P. Zarda, and H. Weinfurter, *Phys. Rev. Lett.* **85**, 290 (2000).
[2] A. Gruber, A. Dräbenstedt, C. Tietz, L. Fleury, J. Wrachtrup, and C. von Borczyskowski, *Science* **276**, 2012 (1997)
[3] A. Beveratos, S. Kuhn, R. Brouri, T. Gacoin, J.-P. Poizat, and P. Grangier, *Eur. Phys. J. D* **18**, 191 (2002).

Significant limitation of defect photoluminescence in diamond arises from the high index of refraction of the bulk material ($n = 2.4$), which makes an efficient extraction of the emitted photons difficult. Refraction at the sample interface leads to a small collection efficiency, limited by total internal reflection and strong optical aberrations. An efficient way to circumvent these problems is to consider the emission of defects in diamond nanocrystals, with size much smaller than the wavelength of the radiated light [4]. The sub-wavelength size of the nanocrystals renders refraction irrelevant and one can then simply treat the color center as a point source radiating in air. Furthermore, the small volume of diamond excited by the pumping laser yields very low background light. Such property is of crucial importance for single-photon emission, since residual background light will contribute to a non-vanishing probability of having more than one photon within the emitted light pulse.

Nanostructured samples are prepared by starting with type Ib synthetic diamond powder (ElementSix, The Netherlands) [3,4]. After irradiation, diamond nanocrystals are dispersed into a polymer solution and then size-selected by centrifugation, with a mean diameter of about 90 nm. The resulting polymer solution containing selected diamond nanocrystals is spin-coated onto the surface of a dielectric mirror, yielding a 30-nm-thick polymer layer which subsequently holds the diamond nanocrystals. The ultra-low fluorescing dielectric structure of the mirror (Layertec, Germany) is optimized to efficiently reflect the photoluminescence of the N-V color center towards the collection optics. We note that the background fluorescence from the mirror dielectric layers is strongly reduced due to photobleaching after a few hours of sample illumination, while the N-V color center emission properties remain unaffected.

Single-photon interferometer with two spatially separated paths

The experiment is based on a 48-meter-long interferometer depicted in the article, very close to the Mach-Zehnder interferometer configuration. A linearly polarized single-photon pulse is sent through a first YVO_4 polarization beamsplitter (BS_{input}) with $45°$ oriented polarization eigenstates. The two S and P linear polarizations at the output of BS_{input} are then spatially separated by 4 mm, sufficient to avoid any overlap between the two beams, since each beam size is about 1 mm. To limit diffraction effects due to open-air propagation along the interferometer, two afocal systems with $\times 5$ magnification are used. After 48 m propagation, equivalent to a time of flight of $\tau_{interf} \simeq 160$ ns, a second polarization beamsplitter (BS′) overlaps the two spatially separated polarizations without recombining the two orthogonally polarized paths of the interferometer. At the output of BS′, the two overlapping polarized channels are sent through a KDP electro-optical modulator (EOM, Linos LM0202, Germany) and a Wollaston prism which separates S and P polarizations. Finally, two silicon avalanche photodiodes (APD) operating in the photon counting regime (Perkin Elmer AQR14) are positioned at the output ports. Depending on the voltage appplied to the EOM ($V = 0$ or $V = V_\pi$), the interferometer is either *closed* or *open* as depicted in Fig.5.

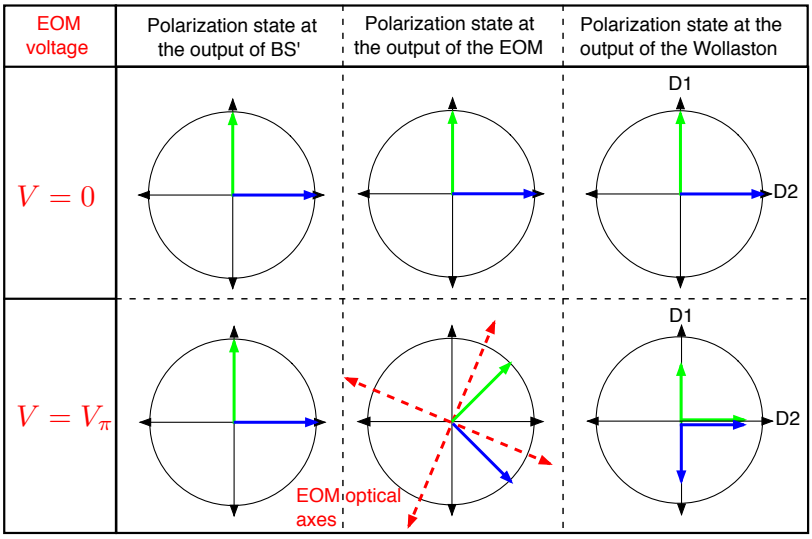

Figure 5: *Polarization states after the second polarization beam splitter BS′ depending on the voltage applied to the EOM. When no voltage is applied, the two polarizations stay unrecombined and the interferometer is open. Detectors D1 and D2, each associated to a given route of the photon along the interferometer, provide a "which-path" information. When the V_π voltage is applied to the EOM, with optical eigenstates oriented at $22.5°$ from the input polarizations, the EOM is equivalent to a half-wave plate which rotates the polarization state by $45°$. The Wollaston prism then mixes the two polarizations and interference appears in the two complementary output ports when the optical path difference between the interfering channels is varied by tilting BS′.*

[4] A. Beveratos, R. Brouri, T. Gacoin, J.-P. Poizat, and P. Grangier, *Phys. Rev. A* **64**, 061802R (2001).

At last, the N-V center photoluminescence is spectrally filtered with a 10 nm FWHM bandwidth centered at 670 nm to avoid any problem of chromatism of the afocal systems and any reduction of interference visibility due to the broadband emission of the N-V color center (see Fig.4-(d)). Finally counting rates of about $700\ \mathrm{count.s}^{-1}$ are measured on each detector in the *open* configuration. The corresponding signal to noise ratio of about 10 is essentially limited by darkcounts of the two APDs, on the order of $60\ \mathrm{count.s}^{-1}$ for each.

Quantum Random Number Generator

To ensure space-like separation between the entrance of the photon into the interferometer and the choice of the performed measurement, the applied voltage on the EOM is randomly chosen in real time, using a Quantum Random Number Generator (QRNG) located at the output of the interferometer. The random numbers are generated from the amplified shotnoise of a white lightbeam. For each clock pulse, i.e. every 238 ns, fast comparison of the amplified shotnoise to the zero level generates a binary random number 0 or 1. As shown on Fig. 6, the autocorrelation function of a random number sequence reveals no significant correlations between different drafts over the time scale relevant for the experiment. We also checked by direct sampling of the amplified shotnoise every 10 ns that its correlation time is approximatively 60 ns. This measurement confirms that choices made at the 4.2 MHz clock rate are uncorrelated.

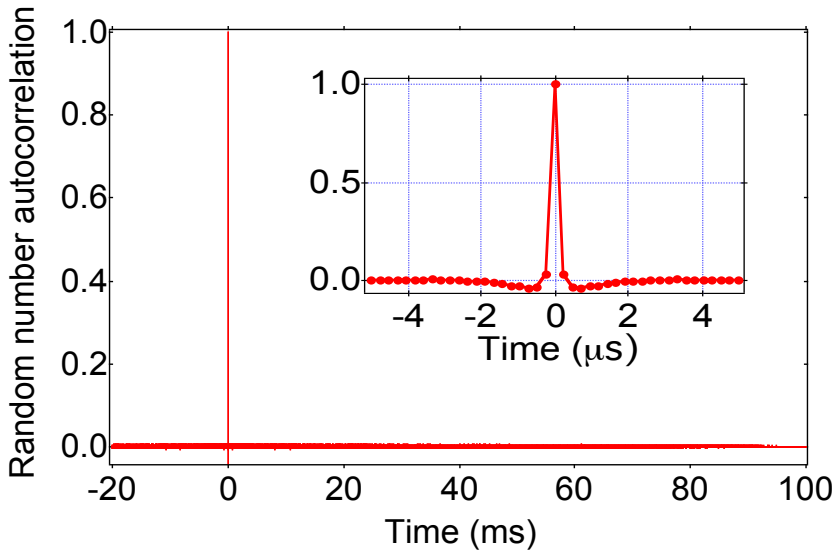

Figure 6: *Normalized autocorrelation function of a* $420\,000$ *random numbers sequence generated at the* 4.2 *MHz clock frequency. Insert displays a zoom of the function close to zero delay. At long time scale no correlation is observed. A small anticorrelation effect of about* 4% *appears at very short time scale (below* 1μs*) presumably due to small oscillations in the amplified output of the shotnoise limited photodetector.*

Timing of the experiment

A small fraction of the pump pulsed laser at 532 nm is used to clock-trigger the experiment with 4.2 MHz repetition rate, corresponding to an excitation of the color center every $\tau_{\mathrm{rep}} = 238$ ns [5]. As depicted on Fig.7, an FPGA programmable circuit generates for each clock pulse the following sequence. First, fast comparison of the amplified shotnoise to the zero level generates a binary random number 0 or 1 which drives the voltage applied to the EOM, switching between the *open* and *closed* configurations. Then a detection gate of duration $\tau_{\mathrm{d}} = 40$ ns is adjusted with appropriate time delays to coincide with the photon arrival on detectors D1 and D2 [6]. The FPGA electronics is programmed in order that the random number generation is realized 160 ns before the detection gate, which corresponds to the time of flight τ_{interf} of the photon inside the interferometer. The QRNG is then drawn simultaneously with the photon emission, within the accuracy of the excited level lifetime τ_{sp} of the N-V center $\tau_{\mathrm{sp}} = 44.5 \pm 0.5$ns (see Fig.4-(b)).

[5] Since the time of flight of the photon in the interferometer τ_{interf} is smaller than the excitation period τ_{rep}, only one single-photon pulse is inside the interferometer at a time.

[6] This gated detection leads to a significant decrease of the effective number of dark counts of D1 and D2.

As shown in the space-time diagram of Fig.7, if the single-photon appears at the very beginning (resp. at the very end) of its time-emission window, it has been inside the interferometer for 85 ns (resp. 40 ns), meaning 25 m (resp.12 m) away from the input beamsplitter, when the EOM voltage starts to commute. Furthermore, such timing ensures that the two events "entering of the photon into the interferometer at $\mathrm{BS_{input}}$" and "choice of the experimental configuration at $\mathrm{BS_{output}}$" are space-like separated in a special relativistic sense, as required in Wheeler's proposal. Indeed, the photon enters the future light-cone of the random choice when it is about at the middle of the interferometer, long after passing $\mathrm{BS_{input}}$.

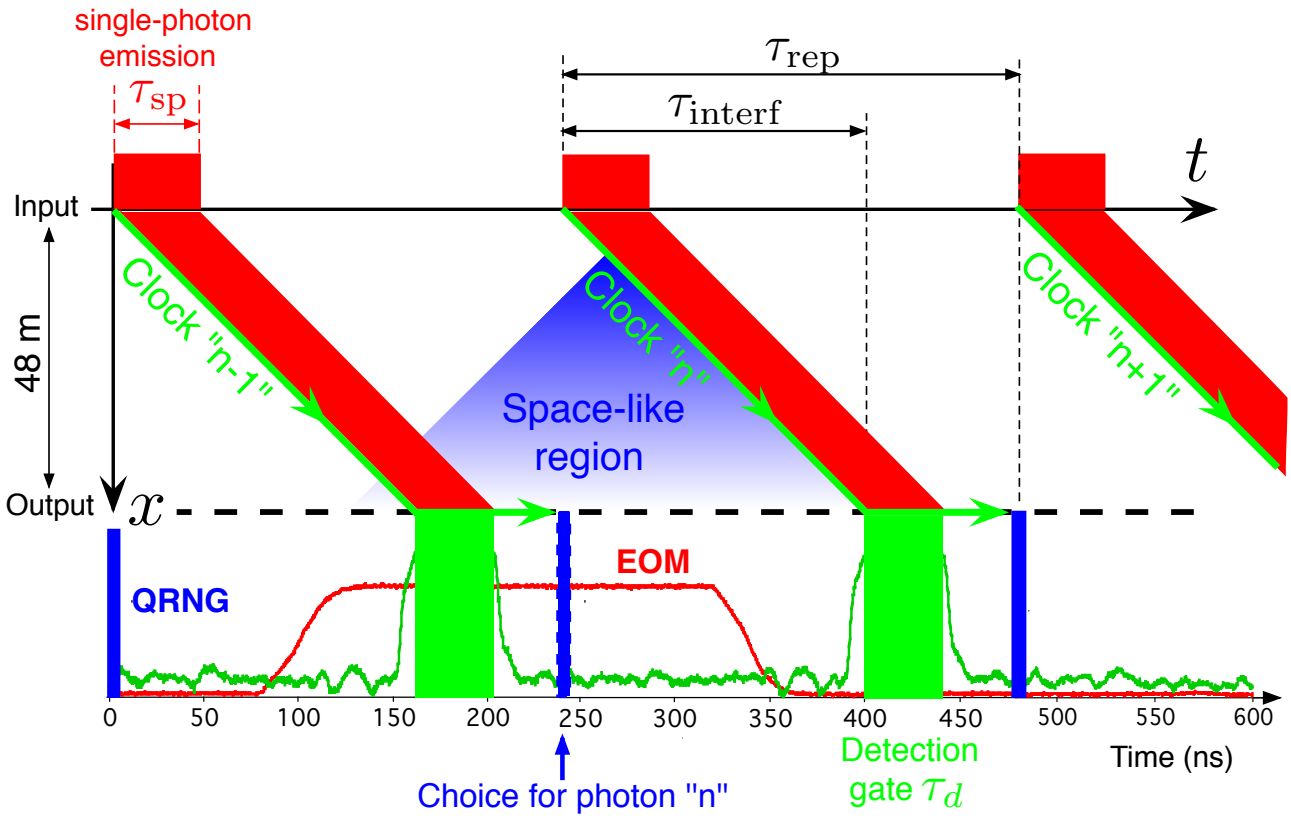

Figure 7: *Timing of the "delayed-choice" experiment, represented as a space-time diagram. Clock pulses of 5 ns duration are generated by detecting part of the pump laser beam at 532 nm. Due to the N-V color center radiative lifetime, the single-photon light pulses are emitted during a gate of duration* $\tau_{\mathrm{sp}} = 44.5 \pm 0.5\mathrm{ns}$. *All the electronics is based on a FPGA programmable circuit which has a few nanoseconds jitter. To account for propagation delays and response time, the measurement applied to photon "n" is synchronised on clock pulse "n-1" which triggers the emission of photon "n-1" (see green bented line corresponding to speed-of-light propagation). The sequence for the measurement applied to photon "n" is done in three steps. First, the binary random number (in blue) which determines the interferometer configuration is generated by the QRNG simultaneously with the trigger of single-photon "n" emission. Then, this binary random number (equal to 0 for photon "n") drives the EOM voltage between* $V = 0$ *and* $V = V_\pi$ *within* 40 *ns, as shown in the figure in red. Finally the single-photon pulse is detected at the outputs ports by D1 or D2, after its time of flight* τ_{interf} *in the interferometer. This detection is done during a gate of duration* $\tau_{\mathrm{d}} = 40$ *ns, generated with three electronic D-latches separated by 20 ns (green line). The blue zone represents the space-like domain associated to the event "entering of photon 'n' into the interferometer". The choice of the open or closed configuration for photon "n" is clearly within that region.*